REPORT DOCUMENTATION PAGE

Form Approved OMB NO. 0704-0188

1. REPORT DATE (DD-MM-YYYY)	2. REPORT TYPE	3. DATES COVERED (From - To)
	New Reprint	-

4. TITLE AND SUBTITLE	5a. CONTRACT NUMBER
Tuning the composition and nanostructure of Pt/Ir films via anodized aluminum oxide templated atomic layer deposition	W911NF-05-1-0177
	5b. GRANT NUMBER
	5c. PROGRAM ELEMENT NUMBER
	611102

6. AUTHORS	5d. PROJECT NUMBER
D. J. Comstock, S. T. Christensen, J. W. Elam, M. J. Pellin, and M. C. Hersam	
	5e. TASK NUMBER
	5f. WORK UNIT NUMBER

7. PERFORMING ORGANIZATION NAMES AND ADDRESSES	8. PERFORMING ORGANIZATION REPORT NUMBER
Northwestern University Chicago Campus Office of Sponsored Research Northwestern University Evanston, IL 60208 -1110	

9. SPONSORING/MONITORING AGENCY NAME(S) AND ADDRESS(ES)	10. SPONSOR/MONITOR'S ACRONYM(S)
U.S. Army Research Office P.O. Box 12211 Research Triangle Park, NC 27709-2211	ARO
	11. SPONSOR/MONITOR'S REPORT NUMBER(S)
	48138-CH-PCS.12

12. DISTRIBUTION AVAILIBILITY STATEMENT

Approved for public release; federal purpose rights

13. SUPPLEMENTARY NOTES

The views, opinions and/or findings contained in this report are those of the author(s) and should not contrued as an official Department of the Army position, policy or decision, unless so designated by other documentation.

14. ABSTRACT

Nanostructured metal films have been widely studied for their roles in sensing, catalysis, and energy storage. In this work, we demonstrate the synthesis of compositionally controlled and nanostructured Pt/Ir films by atomic layer deposition (ALD) into porous anodized aluminum oxide templates. Templated ALD provides advantages over alternative synthesis techniques, including improved film uniformity and conformality as well as atomic-scale control over morphology and composition. Nanostructured Pt ALD films are demonstrated with morphological

15. SUBJECT TERMS

atomic layer deposition, anodized aluminum oxide, platinum, iridium

16. SECURITY CLASSIFICATION OF:			17. LIMITATION OF ABSTRACT	15. NUMBER OF PAGES	19a. NAME OF RESPONSIBLE PERSON
a. REPORT	b. ABSTRACT	c. THIS PAGE	UU		Mark Hersam
UU	UU	UU			19b. TELEPHONE NUMBER 847-491-2696

Standard Form 298 (Rev 8/98)
Prescribed by ANSI Std. Z39.18

Report Title

Tuning the composition and nanostructure of Pt/Ir films via anodized aluminum oxide templated atomic layer deposition

ABSTRACT

Nanostructured metal films have been widely studied for their roles in sensing, catalysis, and energy storage. In this work, we demonstrate the synthesis of compositionally controlled and nanostructured Pt/Ir films by atomic layer deposition (ALD) into porous anodized aluminum oxide templates. Templated ALD provides advantages over alternative synthesis techniques, including improved film uniformity and conformality as well as atomic-scale control over morphology and composition. Nanostructured Pt ALD films are demonstrated with morphological control provided by the Pt precursor exposure time and the number of ALD cycles. With these approaches, Pt films with enhanced surface areas, as characterized by roughness factors as large as 310, have been reproducibility synthesized. Additionally, nanostructured PtIr alloy films of controlled composition and morphology have been demonstrated by templated ALD, with compositions varying systematically from pure Pt to pure Ir. Lastly, the application of nanostructured Pt films to electrochemical sensing applications is demonstrated by the non-enzymatic sensing of glucose.

REPORT DOCUMENTATION PAGE (SF298)
(Continuation Sheet)

Continuation for Block 13

ARO Report Number   48138.12-CH-PCS
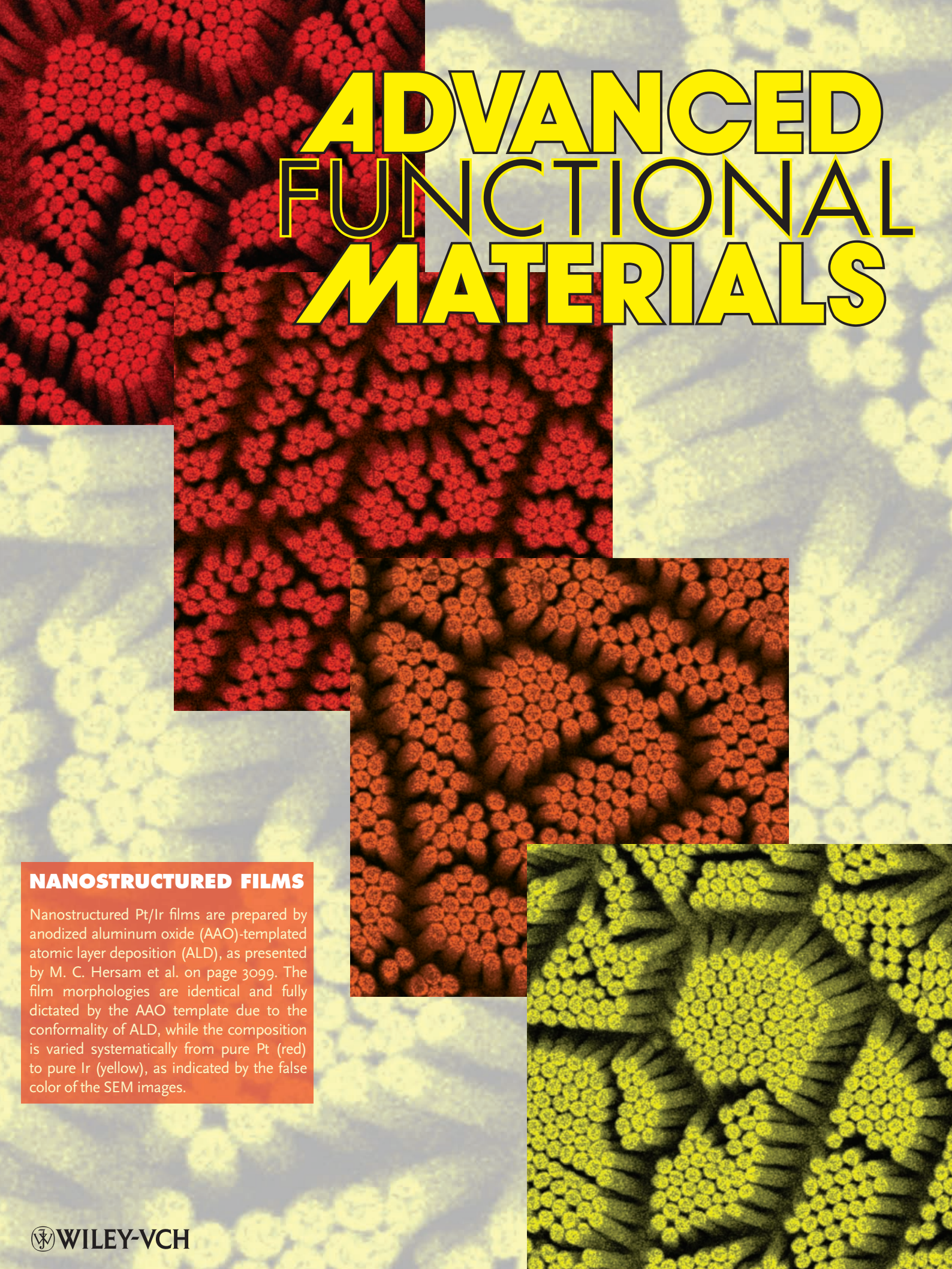Tuning the composition and nanostructure of Pt/   ...

Block 13: Supplementary Note

Approved for public release; federal purpose rights

ADVANCED FUNCTIONAL MATERIALS

NANOSTRUCTURED FILMS

Nanostructured Pt/Ir films are prepared by anodized aluminum oxide (AAO)-templated atomic layer deposition (ALD), as presented by M. C. Hersam et al. on page 3099. The film morphologies are identical and fully dictated by the AAO template due to the conformality of ALD, while the composition is varied systematically from pure Pt (red) to pure Ir (yellow), as indicated by the false color of the SEM images.

Tuning the Composition and Nanostructure of Pt/Ir Films via Anodized Aluminum Oxide Templated Atomic Layer Deposition

By *David J. Comstock, Steven T. Christensen, Jeffrey W. Elam, Michael J. Pellin,* and *Mark C. Hersam**

Nanostructured metal films have been widely studied for their roles in sensing, catalysis, and energy storage. In this work, the synthesis of compositionally controlled and nanostructured Pt/Ir films by atomic layer deposition (ALD) into porous anodized aluminum oxide templates is demonstrated. Templated ALD provides advantages over alternative synthesis techniques, including improved film uniformity and conformality as well as atomic-scale control over morphology and composition. Nanostructured Pt ALD films are demonstrated with morphological control provided by the Pt precursor exposure time and the number of ALD cycles. With these approaches, Pt films with enhanced surface areas, as characterized by roughness factors as large as 310, are reproducibly synthesized. Additionally, nanostructured PtIr alloy films of controlled composition and morphology are demonstrated by templated ALD, with compositions varying systematically from pure Pt to pure Ir. Lastly, the application of nanostructured Pt films to electrochemical sensing applications is demonstrated by the non-enzymatic sensing of glucose.

1. Introduction

Nanostructured metal films with large specific surface areas have found extensive use in a variety of fields including catalysis,[1–4] sensing,[5–7] and energy storage.[8] Among the most common approaches to synthesizing such films is templated deposition,

which utilizes a porous template, such as a liquid-crystal[9,10] or a porous membrane[11,12] to dictate film morphology. Such templated deposition is typically conducted by either electrodeposition or electroless deposition, with mesoporous films and arrays of nanotubes and nanowires having been demonstrated. However, such deposition techniques provide only limited control over film composition and thickness, potentially leading to irreproducible properties and performance for device applications.

Atomic layer deposition (ALD) is an alternative strategy for synthesizing nanostructured metal films with precisely tunable morphology and composition. In its simplest form, ALD employs the iterative introduction of two precursors into a reactor, with each forming a self-terminating monolayer.[13] As each precursor reacts with the surface, film growth proceeds in a monolayer-by-monolayer fashion, yielding highly uniform and conformal films with atomic-scale thickness control. Furthermore, the self-limiting surface chemistry allows nanoporous templates to be uniformly coated on all exposed surfaces. ALD also provides atomic-level compositional control by selecting the appropriate reactants during each ALD cycle. This compositional control has been utilized to deposit a range of materials, including doped materials,[14–16] mixed metal oxides,[17–19] and nanolaminates.[20–22] This combination of attributes makes ALD ideal for the templated synthesis of nanostructured materials, with such templating previously being demonstrated for metal oxide and metal nitride materials[23–25] as well as some metals.[26–29] These templated materials have been utilized for varied applications, including optics,[29] energy storage,[30] and photovoltaics.[31,32]

In this work, templated ALD is utilized to prepare nanostructured Pt/Ir films. Such films have been employed for electrochemical sensing applications, including hydrogen peroxide[33] and non-enzymatic glucose sensing.[34–36] In particular, the synthesis of such nanostructured films is delineated with a focus on the precise tunability of film morphology and composition provided by ALD. The films are quantitatively assessed by scanning electron microscopy (SEM) and X-ray fluorescence (XRF) to verify their morphology and composition, respectively.

[*] Dr. D. J. Comstock, Prof. M. C. Hersam
Department of Materials Science and Engineering
Northwestern University
Evanston, IL 60208 (USA)
E-mail: m-hersam@northwestern.edu

Dr. S. T. Christensen, Dr. J. W. Elam
Energy Systems Division
Argonne National Laboratory
Argonne, IL 60439 (USA)

Dr. M. J. Pellin
Materials Science Division
Argonne National Laboratory
Argonne, IL 60439 (USA)

Dr. M. J. Pellin, Prof. M. C. Hersam
Department of Chemistry
Northwestern University
Evanston, IL 60208 (USA)

Additionally, the films are characterized electrochemically in order to determine their electrochemically active surface area, electrochemical response, and suitability for electrochemical sensing applications.

2. Results and Discussion

2.1. Fabrication of Templated ALD Films

Nanostructured Pt/Ir films are prepared by Pt and Ir ALD into anodized aluminum oxide (AAO) templates. Pt deposition is achieved by alternating exposures to (trimethyl)methylcyclopentadienylplatinum(IV) (Pt(MeCp)Me$_3$) and O$_2$ and occurs at a growth rate of 0.45–0.64 Å cycle^{-1}.[37,38] Ir deposition is achieved by alternating exposures to iridium(III) acetylacetonate (Ir(acac)$_3$) and O$_2$ and occurs at a growth rate of 0.46–0.47 Å cycle^{-1}.[38,39] PtIr alloy films are prepared with precise control over the composition by controlling the ratio of Pt to Ir cycles.[38]

Nanostructured films are prepared using AAO templates. AAO templates exhibit hexagonally-ordered, parallel pores and have been widely used to prepare nanostructures. More importantly, AAO templates provide for nanostructure tunability, as the template dimensions can be systematically varied. This includes varying the interpore spacing,[40–42] pore length, or pore diameter.[25,43] With the flexibility provided by AAO templates, two different ALD templating schemes were utilized, as shown in **Figure 1**. Nanostructured Pt films with tunable morphology are prepared by scheme 1 templating (Figure 1A). Scheme 1

templating employs high aspect ratio (90 nm diameter, 18 μm long) AAO pores (**step 1**) that are too deep for complete infiltration by the Pt film with the ALD conditions utilized (**step 2**). After ALD, the Pt film is retained within the template, and the morphology and roughness factor (R_f) are characterized by SEM and electrochemical measurements. In particular, R_f is calculated as the ratio between the electrochemically active Pt surface area, as measured by hydrogen monolayer adsorption,[44] and the planar, projected area of the Pt film.

Alternatively, compositional tuning of PtIr alloy films is achieved by scheme 2 templating (Figure 1B), with the film morphology controlled by the AAO template. Scheme 2 templating utilizes lower aspect ratio (70 nm diameter, 500 nm long) AAO pores (**step 1**) that are fully and conformally infiltrated by the ALD film (**step 2**). After deposition, the film is inverted and the AAO template is etched away to expose the templated film (**steps 3** and **4**). The morphology of the templated film is confirmed by SEM imaging, and the composition is determined by XRF.

2.2. Morphological Tuning of Templated Pt Films

Typically, the morphology of template-deposited materials is controlled solely by the dimensions (e.g., pore diameter, pore spacing, etc.) of the template. However, ALD provides for additional control over the film morphology by varying the ALD conditions. This tunability allows for the preparation of a wide variety of film morphologies from a fixed template. Specifically, ALD provides for control of the film infiltration depth through the precursor exposure time and the film thickness through the number of ALD cycles.

Morphological tuning is evident in nanostructured Pt films prepared by scheme 1 templating, as shown in **Figure 2** and **Figure 3**. As is typical of ALD films, the Pt films are highly conformal and fully coat both the top surface and the internal pore walls of the template. This conformality is clearly shown by the Pt nanotubes visible in a cross-section of the coated template (Figure 2D). Furthermore, the Pt film is uniform across the sample surface, both in the filling of nearly every pore and the infiltration depth of the pores.

The effect of the Pt(MeCp)Me$_3$ exposure time was studied by depositing Pt films for 400 cycles with exposure times ranging from 1 to 10 s. As shown in Figure 2E, the Pt infiltration depth increases as a function of exposure time, with the infiltration depth exhibiting a square root dependence on exposure time. This dependence is consistent with the diffusion-limited transport of Pt(MeCp)Me$_3$ molecules into the AAO pores[25,45] and provides for reproducible control of the infiltration depth. The film R_f is similarly controlled by exposure time, as it varies predictably with infiltration depth, with a maximum R_f of 227 achieved for an exposure time of 10 s. Larger R_f can be achieved by using even longer Pt(MeCp)Me$_3$ exposure times; however, the square root time dependence makes this approach increasingly impractical for reasonable total deposition times.

The Pt film morphology can also be controlled by varying the number of ALD cycles or film thickness, as shown in Figure 3. Pt films were deposited for 200, 300, and 400 cycles at a constant
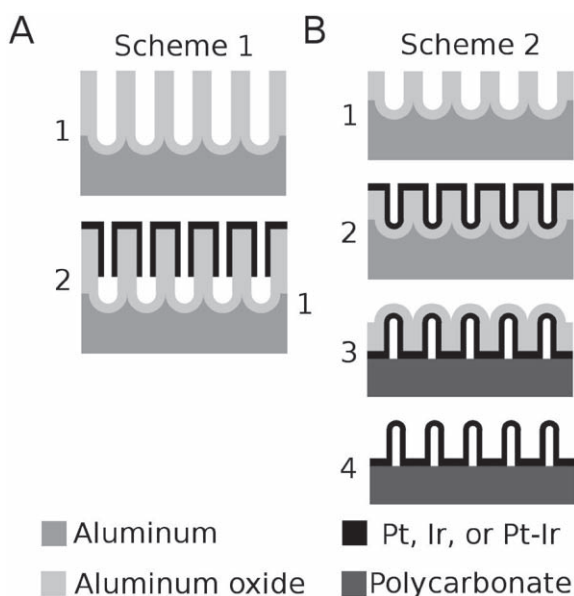
Figure 1. Templating schemes for the synthesis of nanostructured Pt/Ir films by ALD. A) Scheme 1: 1) high-aspect ratio AAO template; 2) ALD deposition that does not fully infiltrate the AAO template. B) Scheme 2: 1) low-aspect ratio AAO template; 2) ALD deposition that fully infiltrates the AAO template; 3) film is inverted, bonded to a polycarbonate substrate, and the aluminum substrate is etched away; 4) AAO template is etched away to expose the templated ALD film.

www.MaterialsViews.com

ADVANCED
FUNCTIONAL
MATERIALS
www.afm-journal.de

FULL PAPER
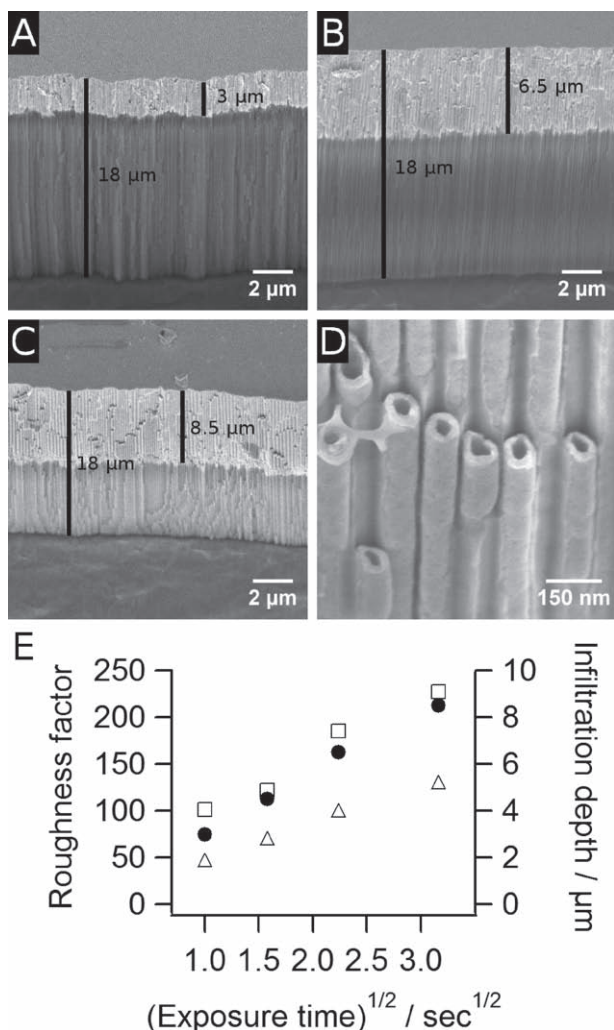
Figure 2. Cross-sectional SEM images of nanostructured Pt films prepared by 400 cycles Pt ALD with $Pt(MeCp)Me_3$ exposure times of A) 1 s, B) 5 s, and C) 10 s. D) Pt nanotube structure observed inside AAO template cross-section. E) Variation in Pt infiltration depth (●), electrochemically measured R_f (□), and geometrically-calculated R_f (△) as a function of $Pt(MeCp)Me_3$ (exposure time)$^{1/2}$.

Figure 3. SEM images of the top surface of nanostructured Pt films deposited for A) 0, B) 200, C) 300, and D) 400 ALD cycles. E) Variation in the diameter of the Pt nanotubes (●), electrochemically measured R_f (□), and geometrically-calculated R_f (△) as a function of the number of Pt ALD cycles.

$Pt(MeCp)Me_3$ exposure time of 10 s to maximize infiltration depth. By reducing the number of ALD cycles, higher surface areas are achieved by preparing Pt nanotubes of increasing internal diameter. This trend is demonstrated by the linear dependence between both pore diameter and R_f on the number of ALD cycles (Figure 3E). As a result, R_f can be increased from 227 to 310 simply by reducing the number of ALD cycles from 400 (~20 nm Pt) to 200 (~10 nm Pt). The increase in R_f with reduced Pt ALD cycles is also significant from a practical perspective, in that higher surface area films and improved performance can be achieved with shorter total deposition times and reduced Pt consumption.

Lastly, it should be noted that the measured R_f for all nanostructured Pt films was consistently larger than the geometrically calculated R_f based upon infiltration depth and pore diameter (Figure 2E and 3E). This desirable enhancement can likely be attributed to interfacial access between the Pt film and the AAO pore wall. In particular, as the surface area measurements are made in acidic solution, the solution may infiltrate between the Pt film and the AAO pore wall, thus also sampling a portion of the Pt nanotube outer surface and effectively increasing the measured surface area.

2.3. Compositional Control of Nanostructured ALD Films

Compositional control is also provided by templated ALD, with nanostructured PtIr alloy films prepared by scheme 2 templating (Figure 1B). Scheme 2 templating relies upon the complete infiltration of the AAO template to produce a film morphology that is fully dictated by the AAO pores and independent of the ALD precursor exposure times. This complete infiltration simplifies the preparation of nanostructured alloy

**ADVANCED
FUNCTIONAL
MATERIALS**

www.afm-journal.de

Materials Views

www.MaterialsViews.com

FULL PAPER

films, as different ALD precursors may have significantly different vapor pressures and molecular weights, both of which control the rate of infiltration into the AAO pores. For example, Ir(acac)$_3$[46] possesses a significantly lower vapor pressure and higher molecular weight compared with Pt(MeCp)Me$_3$,[47] which yields a reduced Ir infiltration depth for a given exposure time. Without precise control over exposure timing and precursor delivery rate, this difference in precursor vapor pressure would yield PtIr alloy films that vary in composition along the axis of the pores for films prepared using scheme 1. On the other hand, the complete infiltration of scheme 2 enables compositionally uniform PtIr alloy nanostructures without the need for precise control over the exposure times.

SEM images and XRF analysis of nanostructured Pt, Ir, and PtIr alloy films are shown in **Figure 4**. As shown, all of the films exhibit identical morphology with 70 nm diameter,
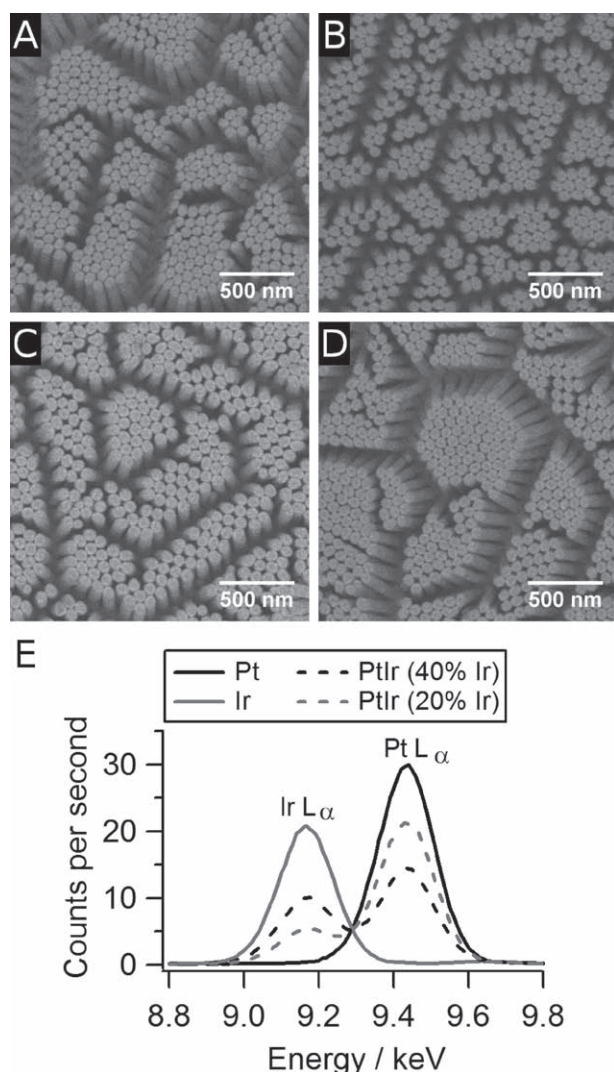
500 nm long closed nanotubes ($R_f = 14$) templated by the AAO pores. The observed clustering of the nanotubes is due to surface tension effects associated with the liquid-phase etching of the AAO template and subsequent drying. In examining the film morphologies, the pure Pt and pure Ir cases are especially important for developing the ALD procedures for alloy deposition, as both alloy components must fully infiltrate the AAO pores. With the 70 nm diameter, 500 nm long AAO pore templates, 10 s Pt(MeCp)Me$_3$ and 20 s Ir(acac)$_3$ exposure times are sufficient for the complete infiltration of both components into the AAO pores.

While the films appear morphologically identical by SEM, the composition varies systematically from pure Pt to pure Ir, as shown in Figure 4E. The composition of the PtIr alloys is controlled by adjusting the ratio of Pt to Ir ALD cycles. In this manner, PtIr alloy films with 20% Ir were prepared with 25% Ir cycles and PtIr alloy films with 40% Ir were prepared with 50% Ir cycles.[38] While the PtIr alloy films exhibit a reduced Ir content relative to the percentage of Ir cycles, this reduction is expected and predictable due to the known reduced growth rate of Ir relative to Pt. Consequently, when the relative growth rates are taken into consideration, PtIr alloy nanostructures of arbitrary composition can be synthesized by controlling the relative number of Pt and Ir ALD cycles. Furthermore, the morphology can be dictated by the AAO template, allowing for fully independent tuning of composition and morphology in nanostructured PtIr alloy films.
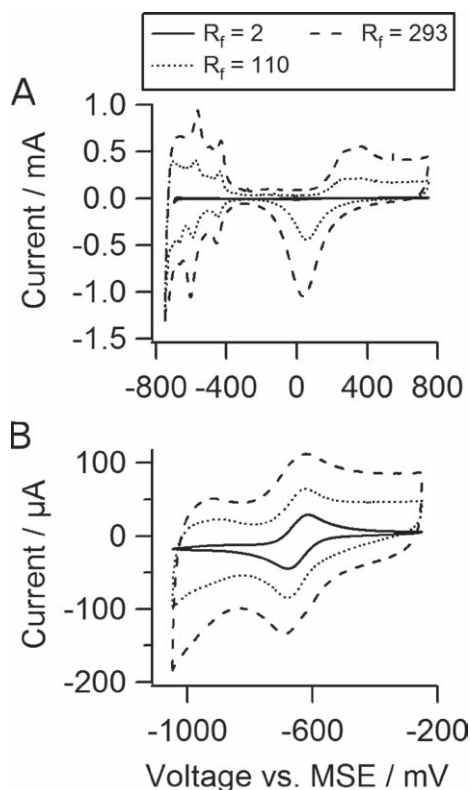
2.4. Electrochemical Response of Nanostructured Pt

The application of the nanostructured Pt films as electrochemical electrodes was investigated by cyclic voltammetry (CV) measurements in acid (1 M H$_2$SO$_4$) and reversible redox mediator (5 mM Ru(NH$_3$)$_6$Cl$_3$, 200 mM K$_2$SO$_4$) solutions, as shown in **Figure 5**. The Pt electrode response in H$_2$SO$_4$ exhibits the characteristic platinum oxidation/reduction response and hydrogen adsorption/desorption response (Figure 5A). As the CV response in H$_2$SO$_4$ is also used to measure R_f, the films exhibit the expected variations with Pt surface area.

On the other hand, the reversible redox mediator response exhibits little dependence on R_f (Figure 5B). While the capacitive background current increases at larger R_f, relatively little change exists in the peak current after accounting for this capacitive background. With a reversible redox mediator, the peak CV current is related to the electrode area by the Randles–Sevcik equation,

$$i_p = 2.69 \times 10^5 n^{3/2} D^{1/2} v^{1/2} c A \tag{1}$$

where n is the number of electrons transferred, D is the diffusion coefficient, v is the scan rate, c is the concentration, and A is the area. Consequently, the invariance of the peak current implies that the Randles–Sevcik electrode area A remains unchanged, even as R_f changes dramatically. This relatively constant electrode area A for nanostructured Pt films is characteristic of a kinetically fast reversible redox mediator. As the mediator reacts with the electrode, it rapidly establishes a depletion region and a diffusion-limited current response. This

Figure 4. SEM images of nanostructured films of A) pure Pt, B) PtIr alloy with 20% Ir, C) PtIr alloy with 40% Ir, and D) pure Ir prepared by templated ALD into 70 nm diameter, 500 nm long AAO pores. E) XRF measurements showing compositional variations between pure Pt, pure Ir, and PtIr alloy films as measured by the Pt L$_\alpha$ and Ir L$_\alpha$ peaks.

www.MaterialsViews.com

ADVANCED
FUNCTIONAL
MATERIALS
www.afm-journal.de

FULL PAPER
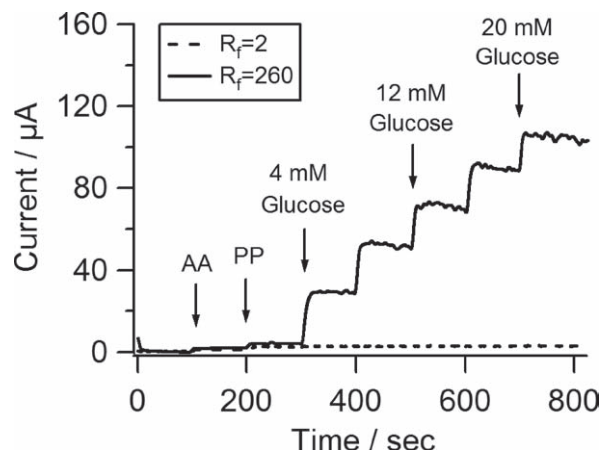
Figure 5. Cyclic voltammetry responses of flat (R_f = 2) and nanostructured (R_f = 110 and R_f = 293) Pt films in A) 1 M H_2SO_4 and B) 5 mM Ru(NH$_3$)Cl$_3$, 200 mM K$_2$SO$_4$.

Figure 6. Amperometric responses of flat (R_f = 2) and nanostructured (R_f = 260) Pt films for glucose sensing. 0.1 mM ascorbic acid (AA), 0.1 mM p-acetamidophenol (PP), and successive 4 mM steps of glucose are added to a constantly stirred solution of 100 mM (pH 7.4) phosphate buffer with 130 mM NaCl.

diffusion-limited response only samples the planar, projected area of the Pt nanostructure and is unable to sample the large internal surface area of the nanostructured Pt film.

2.5. Applications to Glucose Sensing

Nanostructured Pt electrodes are desirable for non-enzymatic glucose sensing due to their high sensitivity and selectivity between glucose and interfering species, such as ascorbic acid (AA) and p-acetamidophenol (PP). This selectivity results from the differing nature of the electrochemical responses between glucose and these interfering species. In particular, the interfering species exhibit fast kinetics and behave much like the reversible redox mediator, with the establishment of a depletion zone and a diffusion-limited response that does not fully sample the large internal surface area of the Pt film. In contrast, glucose exhibits slow kinetics and fully samples the large internal surface area of the Pt film. As a result, nanostructured Pt films exhibit much larger amperometric responses to glucose than to the interfering species.[34]

The amperometric response of a nanostructured Pt film to glucose was measured at a fixed potential of 0.4 V versus Ag/AgCl in a continuously stirred solution of 100 mM phosphate buffer solution (pH 7.4) with 130 mM NaCl. The interfering species, AA and PP, were added at concentrations of 0.1 mM, and glucose was added in steps of 4 mM to a total concentration of

20 mM. As shown in **Figure 6**, the nanostructured Pt film (R_f = 260) exhibits clearly observable glucose sensitivity and selectivity to both AA and PP, while the flat Pt film (R_f = 2) exhibits no detectable sensitivity to glucose.

The nanostructured Pt film shows a near-linear response to glucose in the range 0–20 mM with a sensitivity of 63.8 µA cm^{-2} mM^{-1}. The linear response over this range is desirable, as glucose sensing is most relevant in the physiological range (3–8 mM). This glucose sensitivity also compares well with previous results, with 0.1 µA cm^{-2} mM^{-1} reported for Pt nanotubular arrays,[35] 9.6 µA cm^{-2} mM^{-1} reported for mesoporous Pt,[34] and 93.7 µA cm^{-2} mM^{-1} reported for nanostructured PtIr alloys.[36] However, it should be noted that direct comparisons of sensitivity are difficult due to experimental variations, including solution stirring and R_f. For example, we have observed significant variations in the measured glucose sensitivity as a function of stirring, while increased R_f will also produce enhanced sensitivity. Nevertheless, the linear response and the selectivity provided by these nanostructured Pt films demonstrates their suitability for non-enzymatic glucose sensing and the potential for other templated ALD films for electrochemical sensing applications.

3. Conclusions

Templated ALD is a versatile synthesis technique that enables synthesis of nanostructured Pt/Ir films with precisely controlled morphology and composition. Quantitatively, nanostructured film morphology is demonstrated with R_f values varied from 110 to 310 through controlled Pt(MeCp)Me$_3$ exposure times and the number of ALD cycles. Similarly, precise control over film composition is shown through nanostructured PtIr alloy films with compositions from pure Pt to pure Ir. These nanostructured templated ALD films exhibit predictable electrochemical responses, thus enabling excellent sensitivity and selectivity for non-enzymatic glucose sensing. In addition to

FULL PAPER

enabling applications for nanostructured Pt/Ir films, this work can likely be extended to a diverse range of morphologically and compositionally controlled nanostructured alloy films by employing other ALD compatible precursors.

4. Experimental Section

Materials: Atomic layer deposition (ALD) was conducted using (trimethyl)methylcyclopentadienylplatinum(IV) (Pt(MeCp)Me$_3$) and iridium(III) acetylacetonate (Ir(acac)$_3$) precursors obtained from Strem Chemicals. All other chemicals were obtained from Sigma-Aldrich and used as-received. High-purity aluminum foil (99.999%), perchloric acid, ethanol, oxalic acid, chromic acid, and phosphoric acid were used for anodized aluminum oxide (AAO) template fabrication. Sulfuric acid (H$_2$SO$_4$), hexaammineruthenium(III) chloride (Ru(NH$_3$)Cl$_6$), and potassium sulfate (K$_2$SO$_4$) were used for cyclic voltammetry measurements. D-glucose, l-ascorbic acid, p-acetamidophenol, sodium phosphate dibasic, sodium phosphate monobasic, and sodium chloride were used for amperometric glucose sensing.

Anodized Aluminum Oxide (AAO) Templates: AAO templates were prepared from high-purity aluminum foils. The aluminum foils were first cleaned by sonication in acetone and isopropanol and dried under N$_2$ flow. Prior to anodization, the foils were electropolished to remove surface irregularities. Electropolishing was conducted potentiostatically at 20 V for up to 5 min in a 1:4 v/v perchloric acid:ethanol solution maintained at 5 °C. Highly-ordered AAO templates with 100 nm interpore spacing were prepared by a two-step oxalic acid anodization process.[42,48] The aluminum foil was first anodized at 40 V in 0.3 M oxalic acid at room temperature for at least 4 h. The AAO film was then etched in 6 wt% phosphoric acid, 2 wt% chromic acid at 60 °C for 1 hour, leaving a scalloped aluminum surface to template subsequent anodization. A second anodization was conducted using the same procedure as the first, with the AAO thickness controlled by anodizing time at a growth rate of 9 μm hour^{-1}. Pore diameter was controlled by pore widening in 10% w/v phosphoric acid maintained at 35 °C. Pore widening occurred at a rate of 3 nm min^{-1}.

Atomic Layer Deposition: Pt and Ir ALD were conducted in a viscous flow type reactor.[49] The reactor was maintained at a temperature 300 °C and a pressure of ~1 Torr with 130 sccm N$_2$ carrier gas flow. Pt ALD was conducted by alternating exposures of Pt(MeCp)Me$_3$ and O$_2$, and Ir ALD was conducted by alternating exposures of Ir(acac)$_3$ and O$_2$. The noble metal precursors were contained in heated stainless steel bubblers, with the Pt(MeCp)Me$_3$ bubbler maintained at 50 °C and the Ir(acac)$_3$ bubbler maintained at 170° C. Noble metal precursor exposure was achieved by diverting 60 sccm N$_2$ through the heated bubbler, while O$_2$ exposure was achieved by introducing 60 sccm O$_2$. Each exposure was followed by a purge with N$_2$.

Nanostructured films were prepared by ALD into AAO templates. The AAO templates were sonicated in acetone and isopropanol and dried with N$_2$. After loading into the ALD reactor, the templates were allowed to equilibrate under N$_2$ flow for 10 min and then cleaned by exposure to 400 sccm of 10% ozone in O$_2$ for 10 min. Prior to the metal ALD, a 15 Å ALD Al$_2$O$_3$ film was deposited using alternating exposures to trimethylaluminum and H$_2$O to provide a uniform nucleation layer for Pt and Ir films.

Nanostructured Pt films were prepared by scheme 1 templating (Figure 1A) into 90 nm diameter, 18 μm deep AAO pores. The effect of the Pt(MeCp)Me$_3$ exposure time was studied by depositing Pt films for 400 cycles. Pt(MeCp)Me$_3$ was exposed for 1 to 10 s followed by a purge for 5 s. O$_2$ was exposed for 2 s and followed by a purge for 5 s. The effect of the number of ALD cycles was studied by depositing films for 200, 300, and 400 ALD cycles using a fixed Pt(MeCp)Me$_3$ exposure time of 10 s. After deposition, the Pt film was retained within the template for morphological and electrochemical characterization.

Nanostructured PtIr alloy films were prepared using scheme 2 templating (Figure 1B) into 70 nm diameter, 500 nm deep AAO pores. All PtIr alloy films were deposited for a total of 200 cycles, with the PtIr alloy composition controlled by adjusting the ratio of Pt to Ir cycles. Pt(MeCp)Me$_3$ was exposed for 10 s and purged for 5 s, Ir(acac)$_3$ was exposed for 20 s and purged for 5 s, and O$_2$ was exposed for 2 s and purged for 5 s. After deposition, the films were inverted and epoxy-bonded to a polycarbonate substrate. The aluminum substrate was removed by etching in a solution of CuCl$_2$ and HCl, and the AAO template was removed by etching in 25% w/v KOH. The inverted structure allowed for characterization of the film conformality and the uniformity of pore filling by the Pt and Ir components.

The morphology of the ALD films was characterized by scanning electron microscopy (SEM) using a Hitachi S-4800 SEM. The composition of ALD films was assessed by x-ray fluorescence (XRF) using an energy dispersive Oxford Instruments ED2000 operated at 45 kV and 251 μA with 140 eV energy resolution. The composition of the PtIr alloys was determined by the ratio of Pt L$_\alpha$ and Ir L$_\alpha$ count rates obtained from peak fitting XRF peaks.

Electrochemical Characterization: Electrochemical measurements were performed with a CHI 750C bipotentiostat (CH Instruments, Austin, TX). A three electrode electrochemical cell was used, with the sample as the working electrode, a Pt mesh counter electrode, and either a mercury/mercurous sulfate (MSE) or a silver/silver chloride (Ag/AgCl) reference electrode. The area of the sample exposed to solution was defined by a tape mask with a 0.125 inch diameter hole defining an area of 0.079 cm^2.

The surface area of the Pt film was determined by hydrogen monolayer adsorption in 1 M H$_2$SO$_4$.[44] Measurements were made by cyclic voltammetry (CV) with the voltage swept between –0.75 and 0.75 V vs. MSE at a scan rate of 0.025 V s^{-1}. The measured current was integrated to determine the charge associated with H adsorption. This charge was used to calculate the Pt surface area using a charge density of 210 μC cm^{-2} for adsorption of a H monolayer. The roughness factor, R_f, was calculated as the ratio of the electrochemically-determined Pt surface area to the planar, projected area (0.079 cm^2) of the film.

The electrochemical response of the nanostructured Pt film was assessed by CV measurements with a reversible redox mediator. Measurements were acquired in a solution of 5 mM Ru(NH$_3$)Cl$_6$ with 200 mM K$_2$SO$_4$ supporting electrolyte. The voltage was swept between –1.1 and –0.2 V vs. MSE at a scan rate of 0.025 V s^{-1}.

The glucose sensing capabilities of the nanostructured Pt films were assessed amperometrically. Prior to glucose sensing measurements, the Pt films were electrochemically cleaned by repeated potential cycling between –0.25 and 1.25 V vs. Ag/AgCl at 0.1 V s^{-1} in 1 M H$_2$SO$_4$. Cycling was repeated until a typical voltammogram for clean Pt was observed. Glucose sensing was then conducted in a solution of 100 mM phosphate buffer solution (pH 7.4) with 130 mM NaCl. The Pt film was biased at 0.4 V vs. Ag/AgCl. The solution was stirred continuously. Typical interfering species (i.e., l-ascorbic acid and p-acetamidophenol) were added at concentrations of 0.1 mM while glucose was added stepwise at concentrations of 4 mM to a total concentration of 20 mM.

www.MaterialsViews.com

ADVANCED
FUNCTIONAL
MATERIALS
www.afm-journal.de

FULL PAPER

[1] J. Jiang, A. Kucernak, *J. Electroanal. Chem.* **2002**, *520*, 64.
[2] J. Jiang, A. Kucernak, *J. Electroanal. Chem.* **2002**, *533*, 153.
[3] A. Kucernak, J. Jiang, *Chem. Eng. J.* **2003**, *93*, 81.
[4] D. R. Rolison, *Science.* **2003**, *299*, 1698.
[5] P. N. Bartlett, S. Guerin, *Anal. Chem.* **2003**, *75*, 126.
[6] M. H. Yang, F. L. Qu, Y. S. Lu, Y. He, G. L. Shen, R. Q. Yu, *Biomaterials* **2006**, *27*, 5944.
[7] L. X. Cao, P. S. Yan, K. Sun, D. W. Kirk, *Electroanalysis* **2009**, *21*, 1183.
[8] A. H. Whitehead, J. M. Elliott, J. R. Owen, G. S. Attard, *Chem. Commun.* **1999**, 331.
[9] G. S. Attard, P. N. Bartlett, N. R. B. Coleman, J. M. Elliott, J. R. Owen, J. H. Wang, *Science.* **1997**, *278*, 838.
[10] J. M. Elliott, G. S. Attard, P. N. Bartlett, N. R. B. Coleman, D. A. S. Merckel, J. R. Owen, *Chem. Mater.* **1999**, *11*, 3602.
[11] J. C. Hulteen, C. R. Martin, *J. Mater. Chem.* **1997**, *7*, 1075.
[12] C. R. Martin, *Science.* **1994**, *266*, 1961.
[13] M. Ritala, M. Leskela, in *Handbook of Thin Film Materials*, Vol. *1* (Ed: H. S. Nalwa), Academic Press, San Diego, CA **2001**, 103.
[14] J. W. Elam, D. A. Baker, A. B. F. Martinson, M. J. Pellin, J. T. Hupp, *J. Phys. Chem. C.* **2008**, *112*, 1938.
[15] C. Lee, S. Y. Park, J. Lim, H. W. Kim, *Mater. Lett.* **2007**, *61*, 2495.
[16] J. Niinisto, K. Kukli, T. Sajavaara, M. Ritala, M. Leskela, L. Oberbeck, J. Sundqvist, U. Schroder, *Electrochem. Solid-State Lett.* **2009**, *12*, G1.
[17] M. Vehkamaki, T. Hatanpaa, T. Hanninen, M. Ritala, M. Leskela, *Electrochem. Solid-State Lett.* **1999**, *2*, 504.
[18] J. W. Elam, S. M. George, *Chem. Mater.* **2003**, *15*, 1020.
[19] M. Nieminen, T. Sajavaara, E. Rauhala, M. Putkonen, L. Niinisto, *J. Mater. Chem.* **2001**, *11*, 2340.
[20] C. N. Ginestra, R. Sreenivasan, A. Karthikeyan, S. Ramanathan, P. C. McIntyre, *Electrochem. Solid-State Lett.* **2007**, *10*, B161.
[21] D. H. Triyoso, R. I. Hegde, X. D. Wang, M. W. Stoker, R. Rai, M. E. Ramon, B. E. White, P. J. Tobin, *J. Electrochem. Soc.* **2006**, *153*, G834.
[22] J. W. Elam, Z. A. Sechrist, S. M. George, *Thin Solid Films.* **2002**, *414*, 43.
[23] C. D. Bae, S. Y. Kim, B. Y. Ahn, J. Y. Kim, M. M. Sung, H. J. Shin, *J. Mater. Chem.* **2008**, *18*, 1362.
[24] L. K. Tan, M. A. S. Chong, H. Gao, *J. Phys. Chem. C.* **2008**, *112*, 69.
[25] J. W. Elam, D. Routkevitch, P. P. Mardilovich, S. M. George, *Chem. Mater.* **2003**, *15*, 3507.
[26] W. H. Kim, S. J. Park, J. Y. Son, H. Kim, *Nanotechnology.* **2008**, *19*, 045302.
[27] D. J. Lee, S. S. Yim, K. S. Kim, S. H. Kim, K. B. Kim, *Electrochem. Solid-State Lett.* **2008**, *11*, K61.
[28] M. Daub, M. Knez, U. Gosele, K. Nielsch, *J. Appl. Phys.* **2007**, *101*, 09J111.
[29] K. Jefimovs, J. Laukkanen, T. Vallius, T. Pilvi, M. Ritala, T. Meilahti, M. Kaipiainen, M. Bavdaz, M. Leskela, J. Turunen, *Microelectron. Eng.* **2006**, *83*, 1339.
[30] P. Banerjee, I. Perez, L. Henn-Lecordier, S. B. Lee, G. W. Rubloff, *Nat. Nanotechnol.* **2009**, *4*, 292.
[31] A. B. F. Martinson, J. W. Elam, J. T. Hupp, M. J. Pellin, *Nano Lett.* **2007**, *7*, 2183.
[32] A. B. F. Martinson, T. W. Hamann, M. J. Pellin, J. T. Hupp, *Chem.-Eur. J.* **2008**, *14*, 4458.
[33] S. A. G. Evans, J. M. Elliott, L. M. Andrews, P. N. Bartlett, P. J. Doyle, G. Denuault, *Anal. Chem.* **2002**, *74*, 1322.
[34] S. Park, T. D. Chung, H. C. Kim, *Anal. Chem.* **2003**, *75*, 3046.
[35] J. H. Yuan, K. Wang, X. H. Xia, *Adv. Funct. Mater.* **2005**, *15*, 803.
[36] P. Holt-Hindle, S. Nigro, M. Asmussen, A. C. Chen, *Electrochem. Commun.* **2008**, *10*, 1438.
[37] T. Aaltonen, M. Ritala, T. Sajavaara, J. Keinonen, M. Leskela, *Chem. Mater.* **2003**, *15*, 1924.
[38] S. T. Christensen, J. W. Elam, *Chem. Mater.* **2010**, *22*, 2517.
[39] T. Aaltonen, M. Ritala, V. Sammelselg, M. Leskela, *J. Electrochem. Soc.* **2004**, *151*, G489.
[40] H. Masuda, F. Hasegwa, S. Ono, *J. Electrochem. Soc.* **1997**, *144*, L127.
[41] O. Jessensky, F. Muller, U. Gosele, *Appl. Phys. Lett.* **1998**, *72*, 1173.
[42] H. Masuda, K. Yada, A. Osaka, *Jpn. J. Appl. Phys., Part 2* **1998**, *37*, L1340.
[43] A. W. Ott, J. W. Klaus, J. M. Johnson, S. M. George, K. C. McCarley, J. D. Way, *Chem. Mater.* **1997**, *9*, 707.
[44] S. Trasatti, O. A. Petrii, *J. Electroanal. Chem.* **1992**, *327*, 353.
[45] R. G. Gordon, D. Hausmann, E. Kim, J. Shepard, *Chem. Vap. Deposition* **2003**, *9*, 73.
[46] N. B. Morozova, P. P. Semyannikov, S. V. Sysoev, V. M. Grankin, I. K. Igumenov, *J. Therm. Anal. Calorim.* **2000**, *60*, 489.
[47] Z. L. Xue, H. Thridandam, H. D. Kaesz, R. F. Hicks, *Chem. Mater.* **1992**, *4*, 162.
[48] H. Masuda, K. Fukuda, *Science.* **1995**, *268*, 1466.
[49] J. W. Elam, M. D. Groner, S. M. George, *Rev. Sci. Instrum.* **2002**, *73*, 2981.